In situ evidence that mast cells release mutant NLRP1 in keratoacanthomas from multiple self-healing palmoplantar carcinoma

Alexandra Dobre[1,2], Tudor E. Fertig[1,3]*, Andrei M. Niculae[1,3,4], Adelina M. Cohn[1,5], Antoanela Curici[1,6], Razvan T. Andrei[6,7], Daciana S. Marta[3,8], Victor E. Peteu[3], Roua G. Popescu[9,10], George C. Marinescu[9,10], Gabriela Turcu[1,7,11], Ana M. Forsea[1,2,12], Daniela A. Ion[1], Mihaela Gherghiceanu[1,3]**, Roxana I. Nedelcu[1,11]**

[1] Carol Davila University of Medicine and Pharmacy, Bucharest, Romania

[2] Elias University Emergency Hospital, Dermatology, Bucharest, Romania

[3] Victor Babeş National Institute of Pathology, Bucharest, Romania

[4] Pathology Department, "Dr. Carol Davila" Central Military Emergency University Hospital, Bucharest, Romania

[5] Laboratoire National De Santé, Dudelange, Luxembourg

[6] Synevo Romania, Bucharest, Romania

[7] Colentina Clinical Hospital, Bucharest, Romania

[8] Faculty of Medicine, Titu Maiorescu University, Bucharest, Romania

[9] Asociația Independent Research, Bucharest, Romania

[10] Blue Screen SRL, Bucharest, Romania

[11] Derma 360 Clinic, Bucharest, Romania

[12] Health and Medical University Potsdam, Germany

*Corresponding author: Tudor Emanuel Fertig, +4021 319 2732, Dionisie Lupu 37, Bucharest 030167, emanuel.fertig@umfcd.ro

ABSTRACT

NLRP1 is an inflammasome sensor protein expressed in barrier tissues of humans. Its activation in response to microbes or cellular stress triggers a cascade of molecular events, leading up to IL1β-driven inflammation and pyroptosis. Rare germline mutations of NLRP1 cause its persistent activation, resulting in autoinflammatory syndromes. Multiple self-healing palmoplantar carcinoma (MSPC) is one such syndrome, characterized by the appearance of recurrent keratoacanthomas (KAs) on the palms and soles. Here, we aimed to compare the subcellular localization of mutant NLRP1 in MSPC-associated lesions, to wild-type NLRP1 in non-MSPC KAs and in skin from healthy donors. Using mass spectrometry, immunohistochemistry and immunoelectron tomography, we found that NLRP1 localized to mast cell (MC) granules in all samples, a novel finding which implicates MCs in NLRP1-associated responses in human skin. Moreover, we found that MCs expressing the A66V pathogenic variant of NLRP1 overpopulated MSPC-KAs, infiltrated the epidermis and degranulated, a behavior not seen in other lesions from this study. The released granules had the highest NLRP1 protein content and also contained NLRP3 and IL1β, indicating coexistence of inflammasome pathways within MCs. Taken together, our findings establish cutaneous MCs as a NLRP1 reservoir in health and disease, opening a new area of research in NLRP1-related syndromes.

1. INTRODUCTION

NLRP1 (NLR family pyrin domain containing 1) is a cytosolic sensor protein with a major role in innate immunity. In response to pathogens or other stress signals, NLRP1 can participate in the formation of an intracellular protein complex termed the "inflammasome" [1]. This assembly involves the recruitment of the adapter protein ASC (apoptosis-associated speck-like protein containing a CARD), which facilitates the activation of caspase-1. Once activated, caspase-1 mediates the maturation and secretion of pro-inflammatory cytokines IL-1β and IL-18 and the induction of pyroptosis [2].

In humans, NLRP1 pathogenic variants can lead to a variety of clinical syndromes depending on the affected protein domain, mainly involving the skin, cornea and lungs [3-6]. Of these, multiple self-healing palmoplantar carcinoma (MSPC) is characterized by recurrent keratoacanthomas (KAs) that develop on palmoplantar skin and sporadically on other epithelia lacking hair follicles [7]. Responsible are either one of three germline heterozygous mutations (A54T, A66V, M77V) affecting the pyrin domain (PYD) of NLRP1, causing spontaneous self-oligomerization of the protein, aberrant inflammasome activation and subsequent proliferation of select keratinocytes [7].

Keratinocytes are known as the main NLRP1 reservoir in human skin [7-10], however granulocytes, lymphocytes, macrophages and dendritic cells also express NLRP1[11]. RNA-seq data from the Human Protein Atlas indicates basophils as having the highest potential for NLRP1 protein expression among immune cells [12,13].

Mast cells (MCs) are tissue-resident immune cells of hematopoietic origin, which differentiate from a basophil-MC common progenitor. Although not yet described to contain NLRP1, MCs contain NLRP3 within secretory granules and can produce IL1β following NLRP3 inflammasome activation [14,15]. Mutations of NLRP3 cause it to become constitutively activated in MCs, initiating overproduction of IL1β. This contributes to a spectrum of clinical entities named cryopyrin-associated periodic syndromes (CAPS), in which the skin, joints and central nervous system can be affected [14,16].

We report for the first time that skin MCs harbor NLRP1 within granules. We further show massive and specific degranulation of MCs in different KAs of a MSPC patient with $NLRP1^{A66V}$ and suggest that release of granules containing this hyperactive NLRP1 variant contributes to the pathogenesis of KAs in this syndrome.

72 **2. RESULTS**

73 **2.1. Different skin lesions from a MSPC patient have divergent patterns of inflammasome**
74 **activation**

75 A 49-year-old male with a history of multiple central hyperkeratotic lesions on the palms and
76 soles (**Figure 1a**) in the context of MSPC with NLRP1^{A66V}, presented with symmetrically
77 distributed and well-defined erythematous-squamous plaques, some with erosions and
78 crusting. These initially appeared on the dorsal feet and later spread to the extremities, trunk
79 and head (**Figure 1b**). An infection was ruled out because of unresponsiveness to
80 antibiotics/antifungals and negative PAS staining. Histopathology suggested psoriasis based on
81 the presence of psoriasiform hyperplasia, parakeratosis containing some neutrophiles, thinning
82 of the suprapapillary plates and focal hypogranulosis (**Figure 1c and inset**). However, an
83 overlap with allergic contact dermatitis was suspected due to (a) atypical development and
84 clinical presentation of plaques, (b) positive patch-tests to lanolin alcohol and nickel(II) sulfate
85 hexahydrate, (c) good response of lesions to oral corticotherapy and lanolin-free moisturizers,
86 and (d) lack of recurrence after stopping corticotherapy.

87 MSPC patients characteristically develop palmoplantar KAs and it remains unclear why KAs
88 fail to form on other anatomical regions. The sudden appearance of these extensive atypical
89 hyperkeratotic inflammatory lesions (HL) in our MSPC patient, presented a unique opportunity
90 to compare their lesional microenvironment to that of different plantar KAs from the same
91 individual (biopsied before, concomitantly and after MSPC-HL diagnosis), in an attempt to
92 isolate the etiology of MSPC-KAs.

93 We first asked whether there are differences in inflammasome activation between the two lesion
94 types and we employed MS and IHC to investigate protein expression. As expected, both
95 MSPC-KAs and MSPC-HL showed higher abundance of key inflammasome-associated
96 proteins, compared to healthy skin (**Figure 1d, e**). MS analyses revealed that whereas caspase-
97 1 and IL-18 had similar levels of expression in the two MSPC lesions, ASC was significantly
98 overexpressed in MSPC-HL (**Figure 1d**). This may indicate higher priming of inflammasome
99 pathways and/or accumulation and persistence of stable ASC-based supramolecular complexes
100 in MSPC-HL tissue.

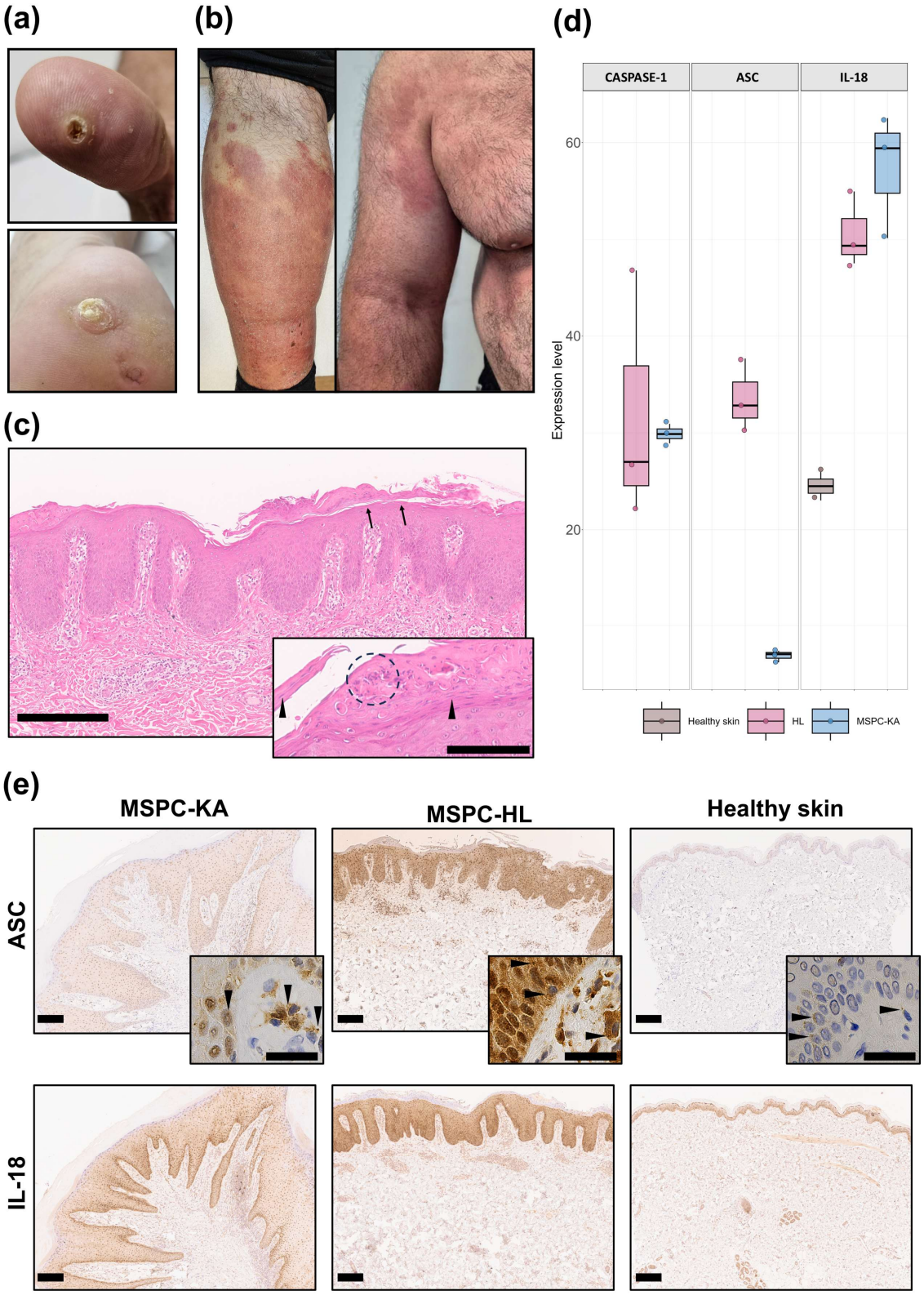
(a)
(b)
(c)
(d)
CASPASE-1
ASC
IL-18
Expression level
60
40
20
Healthy skin
HL
MSPC-KA
(e)
MSPC-KA
MSPC-HL
Healthy skin
ASC
IL-18

101

102 **Figure 1. Inflammasome activation is different between two types of skin lesions from a**
103 **patient with multiple self-healing palmoplantar carcinoma (MSPC).** (**a**) The MSPC patient
104 presented keratoacanthomas (KAs) at different stages of evolution on the palmar and plantar
105 surfaces; (**b**) The MSPC patient suddenly developed a widespread eruption of well-defined
106 erythemato-squamous plaques; (**c**) Hematoxylin and eosin staining (HE, 10x and 20x inset) of
107 an abdominal lesion from the MSPC patient, showed psoriasiform acanthosis with elongation
108 of the rete ridges, thinned suprapapillary plates, hypervascular dermal papillae, neutrophil
109 clusters (circle) in the parakeratotic stratum corneum (arrows heads) and hypogranulosis
110 (arrows); Scale bars are 300 and 100 µm for inset; (**d**) Mass spectrometry (MS) showing higher
111 protein expression levels for caspase-1, apoptosis-associated speck-like protein containing a
112 CARD (ASC) and interleukin-18 (IL-18) the abdominal hyperkeratotic inflammatory lesion
113 (HL) and MSPC-KAs, compared to healthy skin. ASC levels were highest in MSPC-HL, but
114 were below detection levels in healthy skin; (**e**) Spatial distribution of inflammasome-
115 associated proteins ASC (top row and insets) and IL-18 (bottom row) in MSPC lesions and
116 healthy skin. The epidermis of MSPC-HL was strongly positive for ASC and IL-18, which
117 appeared uniformly distributed throughout the cell layers. In MSPC-KAs, both proteins
118 localized to cell clusters in the dermis, but epidermal staining was weaker when compared to
119 MSPC-HL. Granular material suggestive of ASC speck formation is indicated by arrow heads
120 in insets. Scale bars are 200 µm for all images in (e).

121 These complexes (known as "specks") are a hallmark of inflammasome activation and are
122 readily detectable by light microscopy as discrete puncta in the nucleus and cytosol [17; 18].
123 Consistent with MS data, the strongest immunoreactivity for ASC was in the MSPC-HL
124 epidermis. Here, and to a lesser extent in the subjacent dermis, cells exhibited a dispersed
125 punctate pattern indicative of different stages of speck assembly (**Figure 1e, top row and**
126 **inset**). In MSPC-KA lesions, ASC also had a strong, granular signal associated with dermal
127 cell clusters, contrasting with an unexpectedly weak staining of keratinocytes in the overlying
128 epidermis (**Figure 1e, top row and inset**). The differences in staining intensity for IL-18 were
129 less striking, but still favored the epidermis of MSPC-HL, where it appeared uniformly
130 distributed across cell layers. In MSPC-KAs, IL-18 also concentrated to cell clusters in the
131 dermis and in the basal layer of the epidermis (**Figure 1e, bottom row**). These results
132 demonstrated the existence of different hotspots for inflammasome activation in the two MSPC
133 lesions, likely involving site-specific skin cell populations and pathogenic mechanisms.

134 **2.2 MCs accumulate in MSPC-KAs**

135 Given that both MSPC-KAs and MSPC-HL showed increased inflammasome activity but
136 divergent ASC staining patterns, we hypothesized that a cell-specific distribution of
137 $NLRP1^{A66V}$ may at least in part explain the formation of characteristic KAs on palmoplantar
138 skin, but not on skin from other anatomical regions.

139 In IHC, NLRP1 distribution and staining intensity mimicked our spatial data on ASC.
140 Keratinocytes from MSPC-KAs were positive for NLRP1, with a nucleo-cytoplasmic staining
141 pattern and the intensity gradually decreasing towards the upper epidermal layers (**Figure 2a**).
142 Contrary to previous reports [7], the NLRP1 signal was more intense in the dermis than the
143 epidermis, with specific cell populations presenting a granular distribution within the
144 cytoplasm (**Figure 2a, top row inset**). Inversely, $NLRP1^{A66V}$ expression was highest in the
145 epidermis of the MSPC-HL sample, but comparatively reduced in the dermis, mainly clustering
146 around blood vessels (**Figure 2a**). Healthy skin showed the least NLRP1 staining intensity in
147 both epidermis and dermis (**Figure 2a**), although the granular distribution persisted in cells
148 surrounding blood vessels. Positivity of immune cell granules for NLRP1 was confirmed on a
149 human lymph node specimen (**Supplementary Figure S1a**), whereas the isotype control did
150 not bind (**Figure 2a**).

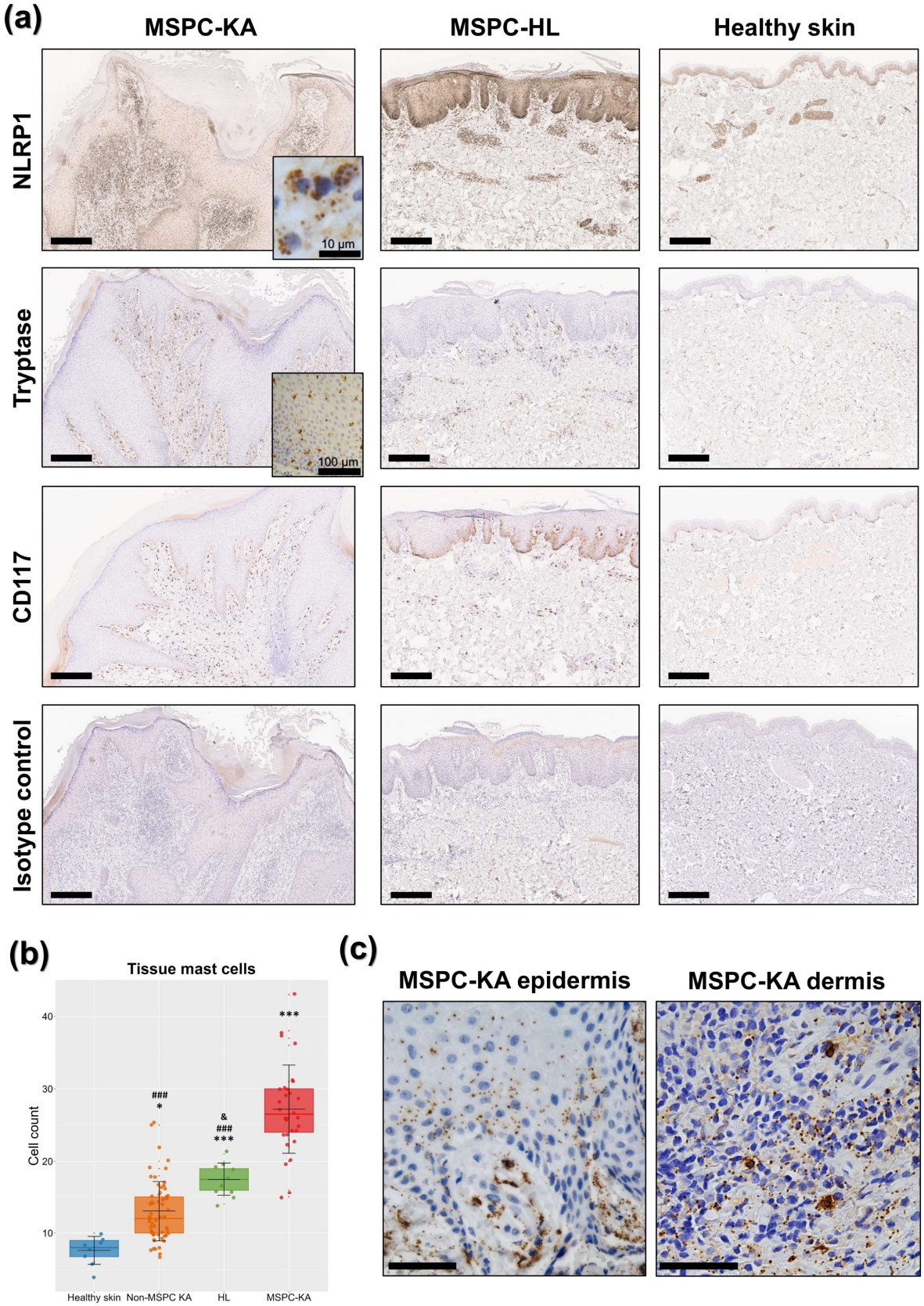
(a)
MSPC-KA
MSPC-HL
Healthy skin
NLRP1
Tryptase
CD117
Isotype control
10 µm
100 µm
(b)
Tissue mast cells
Cell count
40
30
20
10
###
*
&
###
***
***
Healthy skin
Non-MSPC KA
HL
MSPC-KA
(c)
MSPC-KA epidermis
MSPC-KA dermis

152 **Figure 2. Immunohistochemistry of keratoacanthomas (KAs) in multiple self-healing**
153 **palmoplantar carcinoma (MSPC).** (**a**) In MSPC-KAs, NLRP1^{A66V} was more highly
154 expressed in the dermis and was concentrated in cell granules (top row inset, scale bar = 10
155 µm). In an atypical hyperkeratotic inflammatory lesion (HL), NLRP1^{A66V} was overrepresented
156 in the epidermis. CD117 and tryptase staining demonstrated more mast cells (MCs) in MSPC-
157 KAs, including epidermal infiltration (second row inset, scale bar = 100 µm). The isotype
158 control did not bind. Scale bars = 300 µm. (**b**) Quantification of MCs in the analysed samples,
159 presented as means ± standard deviation (SD). Statistical significance is shown against healthy
160 skin—*, MSPC-KA group—#, and the non-MSPC KA group—&, where */& $p < .05$; ***/###
161 $p < .001$. (**c**) MCs in MSPC-KAs were degranulated, with granular material dispersed in
162 epidermis and dermis. Scale bars = 50 µm.

To investigate whether some of the numerous NLRP1-positive cells in the MSPC-KA dermis were MCs, we stained using tryptase and CD117/c-kit (**Figure 2a**). Indeed, KA samples from the MSPC patient had significant MC accumulation (27.2/mm2), above MSPC-HL (17.5/mm2) or healthy skin (7.6/mm2) (**Figure 2b**). In MSPC-KAs but not MSPC-HL, MCs frequently infiltrated epidermal layers (**Figure 2a, second row inset**).

Under higher magnification we further observed that MCs in MSPC-KAs, but not MSPC-HL, were degranulated. Tryptase-positive granular material was widely distributed within connective tissue and taken up in the epidermis, up to the spinous layer (**Figure 2c**). To verify if these are common features of all KAs, we used tryptase staining on six KAs from patients not diagnosed with MSPC (**Supplementary Figure S1b**). As expected [19], these presented MCs in higher numbers (13/mm2) than healthy skin, however below counts in MSPC-KAs and even MSPC-HL (**Figure 2b**). Importantly, we could not identify MC epidermal infiltration, nor MC degranulation, indicating their distinct contribution in MSPC-KA pathogenesis.

The MSPC patient was negative for D816V KIT in whole blood and had normal serum tryptase (<11.4 µg/L), limiting the possibility of MC neoplastic transformation.

Taken together, these results suggest that plantar KAs from a MSPC patient with the $NLRP1^{A66V}$ pathogenic variant have a specific cellular landscape, dominated by high numbers of degranulating MCs, which can infiltrate the epidermis.

2.3 NLRP1 localizes to MC granules

For more precise subcellular localization of NLRP1 we employed immunoelectron microscopy (IEM). Morphologically, most MCs from MSPC-KA were degranulated, ranging from having empty granules and granules fused with the plasma membrane, to complete fragmentation of cells, with release of granular complexes in the extracellular space (**Figure 3a**). By contrast, MCs from MSPC-HL and healthy skin had typical appearance (intact granule architecture, presence of plasma membrane folds) and localized in proximity of blood vessels (**Figure 3b, c**).

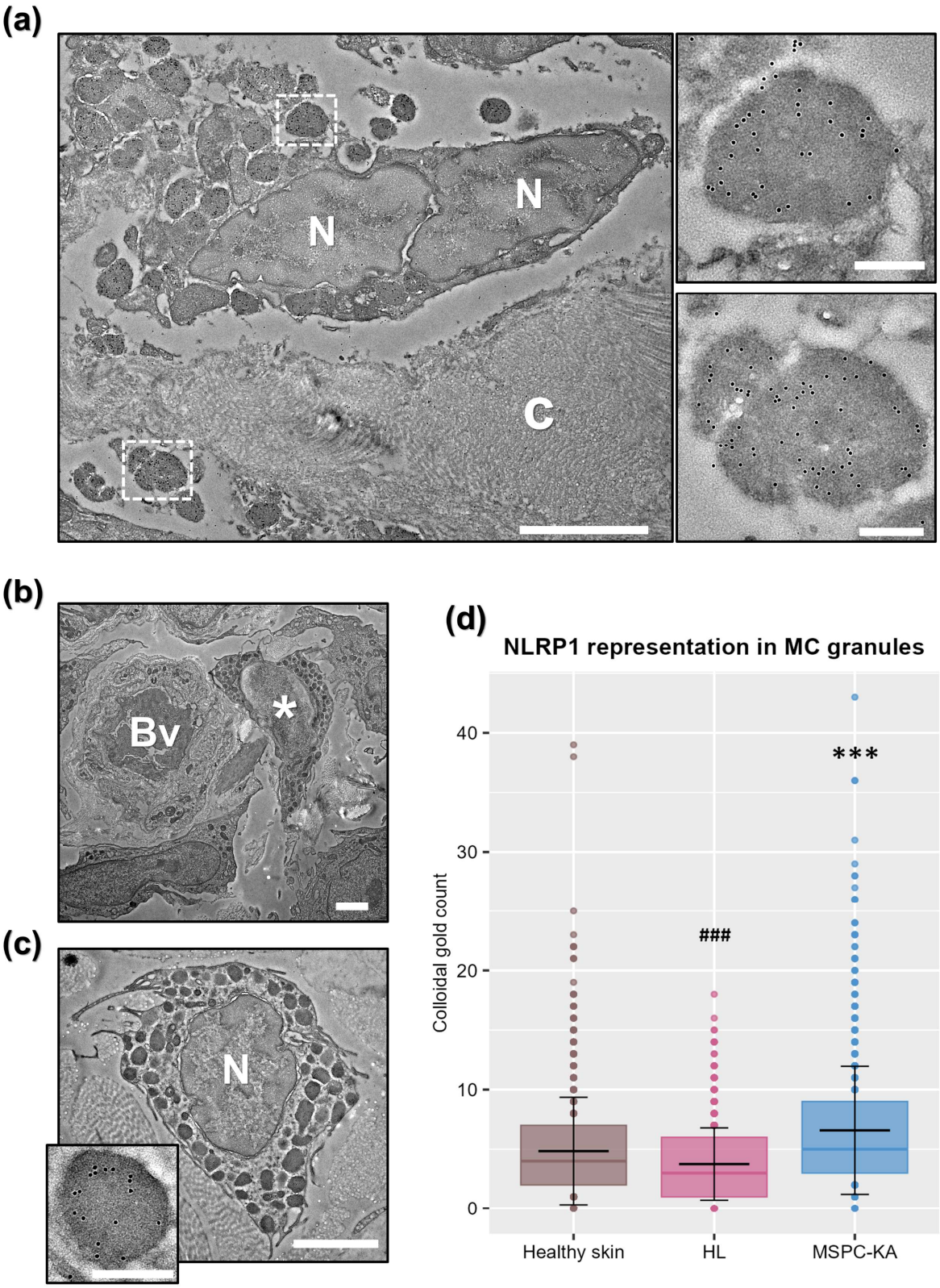
(a)
N
N
C
(b)
Bv
*
(c)
N
(d)
NLRP1 representation in MC granules
Colloidal gold count
0
10
20
30
40
***
###
Healthy skin
HL
MSPC-KA

190 **Figure 3. NLRP1 is ubiquitous in skin mast cell (MC) granules.** (**a**) MCs in
191 keratoacanthomas (KAs) from a multiple self-healing palmoplantar carcinoma (MSPC) patient
192 were degranulated. Scale bar = 2 µm. c - collagen, N - nucleus. MC granules in MSPC-KA
193 presented $NLRP1^{A66V}$ accumulation, as exemplified by higher magnifications of boxed areas.
194 Gold labeling is seen as black dots. Scale bars = 250 nm. (**b**) MCs from an atypical
195 hyperkeratotic inflammatory lesion (HL) were morphologically normal (*) and clustered
196 around blood vessels (Bv). Scale bar = 2 µm. (**c**) Normal MC in healthy skin presenting NLRP1
197 in granules (inset, scale bar = 250 nm). Scale bar = 2 µm. (**d**) Quantification of colloidal gold
198 demonstrated MCs in MSPC-KA had more NLRP1 (means ± standard deviation). Statistical
199 significance is shown against healthy skin—*, and MSPC-KA—#, where ***/### $p < .001$.

200 Using two different, commercially available anti-NLRP1 antibodies, we demonstrated that
201 NLRP1 accumulates in granules of MCs from both lesional and healthy skin, regardless of
202 granule morphology and degranulation status of the cell, indicating NLRP1 is a ubiquitous
203 component of skin MCs (**Figure 3a, c and inset**). By contrast, an isotype control did not bind
204 (**Supplementary Figure S2a**). Next, we asked whether there are differences in MC NLRP1
205 content between samples, so we manually counted and averaged colloidal gold per granule,
206 under identical immunolabeling conditions. In this context, this method of quantification is
207 more precise than western blotting of tissue lysates, as it measures protein content in the
208 subcellular compartment of interest, unbiased by overall representation of MCs in tissue. We
209 found that NLRP1^{A66V} from MSPC-KA was overrepresented compared to NLRP1^{A66V} in
210 MSPC-HL or wild-type NLRP1 in healthy skin (**Figure 3d**), further suggesting MCs may serve
211 as a reservoir of hyper-reactive NLRP1^{A66V} during MSPC-KA pathogenesis.

212 In accordance with IHC, NLRP1 was localized in keratinocytes in all samples, however it
213 unexpectedly clustered around intermediate filaments and desmosomes (**Supplementary**
214 **Figure S2b**).

215 **2.4 NLRP1 and NLRP3 can colocalize in MC granules**

216 MCs are known to contain all components of the NLRP3 inflammasome and to secrete IL1β
217 in a NLRP3-dependent manner [14,15]. Given our finding that NLRP1^{A66V} was present in MC
218 granules from the MSPC patient, we were curious whether it spatially overlapped with NLRP3
219 and if it could therefore share elements of the inflammasome machinery during activation.
220 First, we labeled MSPC-KA against pro-IL1β/IL1β (hereafter IL1β) and found it well
221 represented in both intracellular MC granules and in MC-derived extracellular granular
222 material (**Figure 4a and inset**). This demonstrated that MCs in MSPC-KA secrete this pro-
223 inflammatory cytokine in the extracellular space during degranulation.

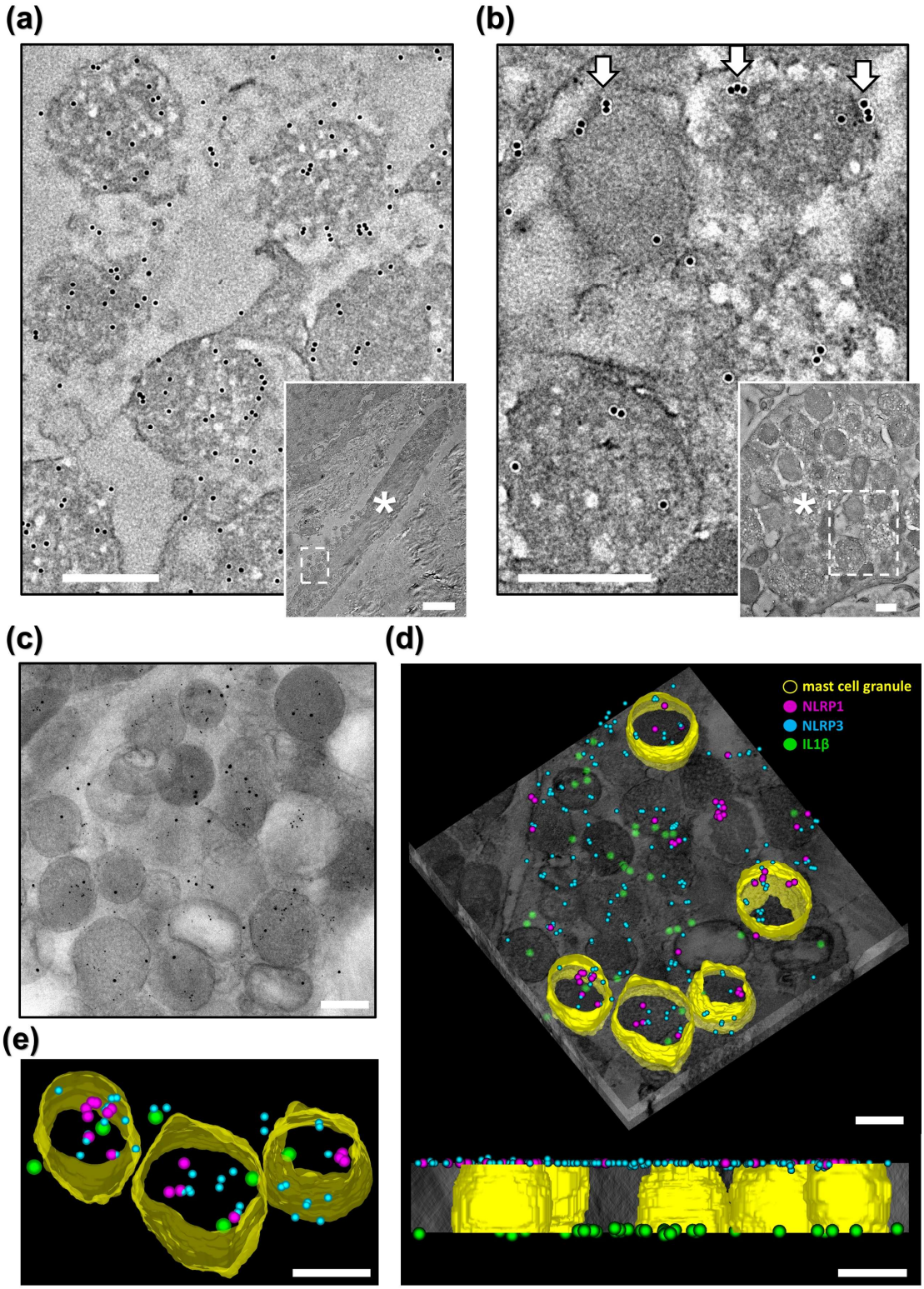

224

225 **Figure 4. NLRP1^{A66V}, NLRP3 and IL1β colocalize to mast cell (MC) granules in a MSPC-**
226 **keratoacanthoma.** (**a**) High magnification of box in inset, confirming pro-IL1β/IL1β in
227 granular material released by a MC (*). (**b**) High magnification of box in inset, showing MCs
228 (*) contain NLRP3, which frequently localized to the periphery of granules (arrows). (**c**)
229 Projection from tomographic tilt series, showing colocalization of gold labels (NLRP1^{A66V},
230 NLRP3, IL1β) in MC granules. (**d, top**) Reconstructed tomogram with superimposed contours
231 of five MC granules (yellow), presenting colocalization of NLRP1^{A66V} (magenta), NLRP3
232 (turquoise) and IL1β (green). (**d, bottom**) Side-view showing distribution of labels to each side
233 of the imaged resin section. (**e**) Detail of segmented MC granules. Scale bar for inset (a) = 2.5
234 µm, all others = 300 nm.

235 Next, we confirmed that some MC granules also contained NLRP3 (**Figure 4b and inset**) and
236 released it during degranulation. NLRP3 was frequently localized at the periphery of
237 cytoplasmic granules and at the plasma membrane in degranulating MCs (**Figure 4b**), in
238 agreement with a recently published study showing a role for NLRP3 in granule exocytosis
239 [20]. Electron tomography on double-labeled sections revealed that NLRP1 and NLRP3 can
240 colocalize to some, but not all MC granules (**Supplementary Figure S2c, d, Supplementary**
241 **Video S1**), raising the possibility of compartmentalization of inflammasome pathways within
242 MCs. Finally, triple-labeling revealed that both sensor proteins can colocalize with IL1β, in
243 both intra- and extracellular MC granules (**Figure 4c-e, Supplementary Video S2**), confirming
244 that multiple inflammasome sensor proteins can simultaneously inhabit MC granules and may
245 act in tandem during activation of MCs in MSPC-KAs.

3. DISCUSSION

Here, we demonstrated that skin MCs can act as a reservoir for NLRP1, a critical but lesser known inflammasome sensor protein. Although novel, this finding is not completely surprising, as MCs express pattern recognition receptors and harbor all components of the NLRP3 inflammasome pathway [15], some of which are also required for NLRP1 inflammasome assembly.

We next showed that MCs are directly involved in the pathogenesis of KAs in a MSPC patient with $NLRP1^{A66V}$. In three different plantar lesions, separated from initial diagnosis by 1, 8 and 10 years, MCs infiltrated the epidermis and $NLRP1^{A66V}$ was released in the dermis and epidermis through widespread MC degranulation. These features were conspicuously absent in a HL specimen from the abdominal skin of the same MSPC patient or in KAs from 6 non-MSPC patients.

The activation of MCs in MSPC-KAs may be a response to NLRP1-inflammasome activation in local keratinocytes, which would then release pro-inflammatory factors. However, this is difficult to reconcile with two key findings: (1) that the highest intensity of ASC and NLRP1 staining were in the MSPC-HL epidermis, where keratinocytes also express the hyperactive $NLRP1^{A66V}$, yet do not form KAs, and (2) that compared to healthy skin, MSPC-HL presented high numbers of MCs prone to activation by keratinocyte inflammatory cues, but these MCs had normal morphology.

Alternatively, the particular MC behaviour in the plantar skin of this MSPC patient may be the result of intrinsic NLRP1-inflammasome activation in response to yet unknown triggers. Activation of select MC clusters and release of granular material would induce keratinocyte inflammatory responses, increasing MC recruitment within the lesion.

In support of this, we showed that MC granular material spread throughout the basal and spinous layers of MSPC-KAs. These granules had higher NLRP1 content than equivalents in MSPC-HL and healthy skin and also harbored NLRP3 and IL1β. The latter can be converted to its active form within intact granules via the NLRP1 and NLRP3 inflammasome pathways, but also in the extracellular environment by endogenous proteases [20,21], thereby driving keratinocyte proliferation [21]. Additionally, tryptase released during MC degranulation can cleave protease activated receptor 2 (PAR-2) on keratinocytes [22], stimulating non-specific particle uptake through phagocytosis [23]. In MSPC-KAs, this would allow enrichment of keratinocytes with components of the NLRP1/NLRP3 inflammasome pathways and other

278 granule components known to stimulate keratinocyte proliferation (e.g. histamine, serotonin
279 and keratinocyte growth factor) [24,25]. The pro-inflammatory activity of extracellular sensor
280 proteins has been previously demonstrated for ASC and mutant NLRP3 oligomers. After being
281 internalized by macrophages through phagocytosis, these complexes can induce ASC
282 aggregation, caspase-1 activation and IL-1β release [26]. The characteristic palmoplantar
283 epidermal hyperplasia in MSPC-KAs may therefore be conditioned by aberrant, NLRP1-
284 dependent activity of tissue-resident MCs.

285 This study has two important limitations. First, in absence of functional studies, we cannot
286 definitively ascertain whether MC degranulation is a prerequisite for MSPC-KA formation, or
287 if it is a local response mechanism which merely modulates lesion development. As murine
288 NLRP1 lacks the PYD domain [7], an in vitro experiment would be required, involving co-
289 culture of human keratinocytes with MCs expressing mutant NLRP1. Second, because we
290 could only include a single MSPC patient, carrying the NLRP1^{A66V} pathogenic variant, we are
291 unable to extrapolate our findings to other MSPC variants. This is further hindered by the rarity
292 of these diseases, with only 5 MSPC families known worldwide [27].

293 In summary, we showed for the first time that NLRP1 is a component of skin MC granules and
294 can colocalize with NLRP3 and IL1β, indicating that MCs have more avenues for
295 inflammasome activation than previously known. We also showed that when MCs from plantar
296 skin express NLRP1^{A66V}, they proliferate, infiltrate the epidermis and degranulate, contributing
297 to the pathogenesis of KAs in this variant of MSPC. This opens a new area of research in
298 NLRP1-related syndromes and, if confirmed in other patients, would translate clinically to
299 accessible therapies targeting MC activity.

300 **4. MATERIALS AND METHODS**

301 **4.1. Patients and samples**

302 All subjects gave written informed consent prior to biopsy. The MSPC patient included here
303 was diagnosed and genetically characterized in a previous study [7]. Four samples were
304 collected from this patient: three different KAs from plantar regions (in 2016, 2023 and 2025)
305 and a sample from an atypical hyperkeratotic inflammatory lesion (HL) on the abdomen (in
306 2023). Biopsies were collected from the elbow region of two clinically healthy volunteers. The
307 study included 6 archived formalin-fixed paraffin-embedded (FFPE) KA specimens from
308 different patients with no clinical history of MSPC. Human lymph node and tonsil FFPE
309 specimens were included as NLRP1 and ASC positive controls. This study was performed in
310 conformity with the Declaration of Helsinki and received approval from the ethics committees
311 at Victor Babeș National Institute of Pathology and Elias University Emergency Hospital,
312 Bucharest, Romania.

313 **4.2. Light microscopy and immunohistochemistry**

314 Hematoxylin-eosin was done by routine protocol. Immunohistochemistry (IHC) with the
315 primary antibody of interest (**Supplementary Table S1**) was done using an Autostainer Link
316 48, following manufacturer specifications (Dako, Agilent Technology, US). An isotype control
317 and omission of primary antibody were used to verify non-specific binding. Digital slides were
318 generated using an automated slide scanner (Aperio AT2, Leica Biosystems, US). Images were
319 processed by Contrast Limited Adaptive Histogram Equalization (CLAHE) in Fiji [28], using
320 the same settings for each type of staining.

321 **4.3. Mass spectrometry**

322 Biopsies were collected in cold PBS, then 50 mg from each sample was disrupted in a Mini-
323 Beadbeater (Biospec, US). Samples were then centrifuged for 20 minutes at 18,000 g and the
324 protein concentration from the supernatant was quantified by Bradford assay. A total of 50 µg
325 of protein containing supernatant was diluted with urea buffer to the final volume of 40 µL,
326 followed by the addition of 25 µL of 100 mM DTT and incubation at room temperature for 60
327 minutes. The sample was then alkylated with 26.25 µL of 300 mM iodoacetamide and kept in
328 the dark at room temperature for an additional 90 minutes followed by a quenching reaction

329 with 50 µL of DTT 100mM at room temperature for 60 minutes. The reaction mix was finally
330 diluted to 500 µL with 50 mM ammonium bicarbonate, followed by addition of trypsin (1 µg
331 /µL; Trypsin Gold, V528A, Promega, US) at a 1:50 enzyme-to-substrate ratio, with incubation
332 at 37°C for 16 hours. The reaction was stopped by adding 3 µL of formic acid. Peptides were
333 cleaned up using solid phase extraction (MonoSpin C18, GL Sciences, Japan), dried at speed-
334 vac and rehydrated to 2 µg/µL using 5% ACN + 0.1% HCOOH. Peptide concentration was
335 measured using NanoDrop 1000 (Thermo Fisher Scientific, US). From each sample, 5 µg
336 peptides were loaded into nanoACQUITY UPLC system (Waters, US) and separated using an
337 Eksigent 5C18-CL-120 (300 µM ID, 150 mm length) column coupled with a TripleTOF 5600+
338 mass spectrometer (both AB Sciex, USA). Peptide samples (5 µg) were injected using Solvent
339 A (0.1% formic acid) and separated on a 5-90% gradient Solvent B (0.1% formic acid in
340 acetonitrile) over 90 minutes, at a flow rate of 5 µL/min, with the column maintained at 55°C.
341 Each sample underwent three replicate runs. Mass spectrometric (MS) analysis was carried out
342 using electrospray ionization in positive mode, with a spray voltage of 5500 V and a source
343 temperature of 200°C. Data acquisition was performed on a TripleTOF 5600+ system in DIA
344 SWATH-MS mode, with 64 variable isolation windows. The MS1 survey scans covered an m/z
345 range of 400–1250, while MS2 spectra were collected in high-sensitivity mode from 100 to
346 2000 m/z. The accumulation period was set to 0.049 s, and ions were scanned within 55 ms
347 windows in high-sensitivity mode, giving a total cycle time of 3.5 s. Peptide and protein
348 identification were performed using PeakView 2.2, Skyline 22.2.0.255 and DIA-NN 1.9.

349 **4.4. Immunoelectron microscopy**

350 Biopsies were fixed in a solution comprising 4% paraformaldehyde, 0.5% glutaraldehyde, and
351 1.4% sucrose (pH 7.4), then embedded in London Resin White (LR White, Agar Scientific,
352 UK). Ultra-thin sections were mounted on formvar and carbon-coated nickel grids, then
353 incubated with the primary antibody of interest (**Supplementary Table S1**) and a gold-
354 conjugated secondary antibody at 1:50 dilution (Aurion, The Netherlands). Negative controls
355 had primary antibodies omitted and an isotype control was used to exclude nonspecific binding
356 to MC Fc receptors. A blocking solution for goat antibodies was used to reduce nonspecific
357 binding (Aurion, The Netherlands). Imaging was done using a 4×4k Ceta camera, on a Talos
358 200C transmission electron microscope (Thermo Fisher Scientific, US).

359 **4.5. Immunoelectron tomography**

360 LR White sections (300 nm) were adhered to nickel grids precoated with 0.01% poly-L-lysine
361 and without formvar or carbon. For double-labeling, grids were incubated on each side,
362 consecutively, with two primary antibodies raised in different species (mouse and rabbit,
363 **Supplementary Table S1**). For triple-labeling, grids were incubated on one side with a mixture
364 of two antibodies raised in different species (mouse and rabbit, **Supplementary Table S1**),
365 then either a rabbit or mouse primary antibody was used on the other side. Secondary antibodies
366 had different colloidal gold diameters for each target (6, 10 and 15 nm, Aurion, The
367 Netherlands). Absence of cross-contamination between section faces was verified by
368 immunolabeling control grids on one side, while the other side was incubated with PBS.
369 Acquisition of single axis tilt series and tomographical reconstruction and segmentation in
370 IMOD-eTomo [29], were done as described elsewhere [30].

371 **4.6. Data analyses**

372 Quantification of MCs was performed on tissue sections stained for tryptase. For each case,
373 tryptase-positive cells were manually counted in ten consecutive high-power fields (HPF, 40×
374 objective), starting from a hotspot. Each experimental group included approximately 27
375 observations. To quantify the NLRP1 content of MC granules, cells were first identified on
376 randomly selected ultrathin sections from the MSPC and healthy skin specimens,
377 immunolabeled under identical conditions. Entire MCs were imaged, then colloidal gold was
378 counted on all granules of each cell. Each experimental group included approximately 1,058
379 observations.

380 Statistical analyses were performed using one-way ANOVA, followed by Tukey's post hoc test
381 for pairwise comparisons between groups. Statistical significance is presented only for
382 comparisons with p-values $< .05$. The post hoc statistical power for the applied tests was 1.
383 Graphical representations were generated using R 4.4.1.

REFERENCES

1. Martinon F, Burns K, Tschopp J. The Inflammasome: A molecular platform triggering activation of inflammatory caspases and processing of proIL-β. Mol Cell [Internet]. 2002 [cited 2025 Jun 21];10:417–26. Available from: https://pubmed.ncbi.nlm.nih.gov/12191486/
2. Bauernfried S, Hornung V. Human NLRP1: From the shadows to center stage. Journal of Experimental Medicine [Internet]. 2021 [cited 2025 Jun 21];219. Available from: https://doi.org/10.1084/jem.20211405
3. Barry K, Murphy C, Mansell A. NLRP1- A CINDERELLA STORY: a perspective of recent advances in NLRP1 and the questions they raise. Commun Biol [Internet]. 2023 [cited 2025 Jun 21];6:1–7. Available from: https://www.nature.com/articles/s42003-023-05684-3
4. Mitchell PS, Sandstrom A, Vance RE. The NLRP1 inflammasome: new mechanistic insights and unresolved mysteries. Curr Opin Immunol [Internet]. 2019 [cited 2025 Jun 21];60:37–45. Available from: https://pubmed.ncbi.nlm.nih.gov/31121538/
5. Burian M, Schmidt MF, Yazdi AS. The NLRP1 inflammasome in skin diseases. Front Immunol. 2023;14:1111611.
6. Calabrese L, Fiocco Z, Mellett M, Aoki R, Rubegni P, et al. Role of the NLRP1 inflammasome in skin cancer and inflammatory skin diseases. British Journal of Dermatology [Internet]. 2024 [cited 2025 Jun 21];190:305–15. Available from: https://pubmed.ncbi.nlm.nih.gov/37889986/
7. Zhong FL, Mamaı¨, M, Sborgi L, Saad A, Hiller S, et al. Germline NLRP1 Mutations Cause Skin Inflammatory and Cancer Susceptibility Syndromes via Inflammasome Activation. Cell [Internet]. 2016 [cited 2024 Apr 18];167:187–202. Available from: http://dx.doi.org/10.1016/j.cell.2016.09.001
8. Sand J, Haertel E, Biedermann T, Contassot E, Reichmann E, et al. Expression of inflammasome proteins and inflammasome activation occurs in human, but not in murine keratinocytes. Cell Death Dis [Internet]. 2018 [cited 2025 Jun 21];9:1–14. Available from: https://www.nature.com/articles/s41419-017-0009-4
9. Feldmeyer L, Keller M, Niklaus G, Hohl D, Werner S, Beer HD. The Inflammasome Mediates UVB-Induced Activation and Secretion of Interleukin-1β by Keratinocytes. Current Biology [Internet]. 2007 [cited 2025 Jun 21];17:1140–5. Available from: https://www.sciencedirect.com/science/article/pii/S0960982207015084
10. Marie J, Kovacs D, Pain C, Jouary T, Cota C, et al. Inflammasome activation and vitiligo/nonsegmental vitiligo progression. Br J Dermatol. 2014 Apr;170(4):816-23. doi: 10.1111/bjd.12691. PMID: 24734946.
11. Kummer JA, Broekhuizen R, Everett H, Agostini L, Kuijk L, et al. Inflammasome components NALP 1 and 3 show distinct but separate expression profiles in human tissues suggesting a site-specific role in the inflammatory response. Journal of Histochemistry and Cytochemistry [Internet]. 2007 [cited 2025 Jun 21];55:443–52. Available from: https://pubmed.ncbi.nlm.nih.gov/17164409/
12. Karlsson M, Zhang C, Méar L, Zhong W, Digre A, et al. A single–cell type transcriptomics map of human tissues. Sci Adv [Internet]. 2021 [cited 2025 Jun 21];7. Available from: https://pubmed.ncbi.nlm.nih.gov/34321199/
13. The Human Protein Atlas [Internet]. [cited 2025 Jun 21]. Available from: www.proteinatlas.org
14. Nakamura Y, Kambe N, Saito M, Nishikomori R, Kim YG, et al. Mast cells mediate neutrophil recruitment and vascular leakage through the NLRP3 inflammasome in histamine-independent urticaria. Journal of Experimental Medicine [Internet]. 2009 [cited 2025 Jul 16];206:1037–46. Available from: https://pubmed.ncbi.nlm.nih.gov/19364881/
15. Bonnekoh H, Scheffel J, Kambe N, Krause K. The role of mast cells in autoinflammation. Immunol Rev [Internet]. 2018 [cited 2025 Apr 22];282:265–75. Available from: https://pubmed.ncbi.nlm.nih.gov/29431217/
16. Nakamura Y, Franchi L, Kambe N, Meng G, Strober W, Núñez G. Critical Role for Mast Cells in Interleukin-1β-Driven Skin Inflammation Associated with an Activating Mutation in the Nlrp3 Protein. Immunity [Internet]. 2012 [cited 2025 Jun 21];37:85–95. Available from: https://pubmed.ncbi.nlm.nih.gov/22819042/
17. Smatlik N, Drexler SK, Burian M, Röcken M, Yazdi AS. ASC Speck Formation after Inflammasome Activation in Primary Human Keratinocytes. Oxid Med Cell Longev. 2021 Nov 5;2021:7914829. doi: 10.1155/2021/7914829. PMID: 34777694; PMCID: PMC8589508.

18. Bryan NB, Dorfleutner A, Rojanasakul Y, Stehlik C. Activation of inflammasomes requires intracellular redistribution of the apoptotic speck-like protein containing a caspase recruitment domain. J Immunol. 2009 Mar 1;182(5):3173-82. doi: 10.4049/jimmunol.0802367. PMID: 19234215; PMCID: PMC2652671.

19. Aguiar ALM, Martins CJ, Meuser-Batista M, Carvalho V, Barreto EO, et al. A case of keratoacanthoma centrifugum marginatum with a curious mast cell accumulation at tumour sites [28]. Journal of the European Academy of Dermatology and Venereology [Internet]. 2007 [cited 2025 Apr 26];21:429–31. Available from: https://pubmed.ncbi.nlm.nih.gov/17309493/

20. Mencarelli, A., Bist, P., Choi, H.W. et al. Anaphylactic degranulation by mast cells requires the mobilization of inflammasome components. Nat Immunol 25, 693–702 (2024). https://doi.org/10.1038/s41590-024-01788-y

21. Macleod T, Berekmeri A, Bridgewood C, Stacey M, McGonagle D, Wittmann M. The Immunological Impact of IL-1 Family Cytokines on the Epidermal Barrier. Front Immunol [Internet]. 2021 [cited 2025 Jul 16];12:808012. Available from: www.frontiersin.org

22. Santulli RJ, Derian CK, Darrow AL, Tomko KA, Eckardt AJ, et al. Evidence for the presence of a protease-activated receptor distinct from the thrombin receptor in human keratinocytes. Proc Natl Acad Sci U S A [Internet]. 1995 [cited 2025 Jun 21];92:9151–5. Available from: /doi/pdf/10.1073/pnas.92.20.9151?download=true

23. Benito-Martínez S, Salavessa L, Raposo G, Marks MS, Delevoye C. Melanin Transfer and Fate within Keratinocytes in Human Skin Pigmentation. Integr Comp Biol [Internet]. 2021 [cited 2025 Jun 21];61:1546–55. Available from: https://pubmed.ncbi.nlm.nih.gov/34021340/

24. Maurer M, Opitz M, Henz BM, Paus R. The mast cell products histamine and serotonin stimulate and TNF-α inhibits the proliferation of murine epidermal keratinocytes in situ. J Dermatol Sci [Internet]. 1997 [cited 2025 Jun 21];16:79–84. Available from: https://pubmed.ncbi.nlm.nih.gov/9438912/

25. Cho KA, Kim HJ, Kim YH, Park M, Woo SY. Dexamethasone Promotes Keratinocyte Proliferation by Triggering Keratinocyte Growth Factor in Mast Cells. Int Arch Allergy Immunol [Internet]. 2019 [cited 2025 Jun 21];179:53–61. Available from: https://pubmed.ncbi.nlm.nih.gov/30909282/

26. Baroja-Mazo, A., Martín-Sánchez, F., Gomez, A. et al. The NLRP3 inflammasome is released as a particulate danger signal that amplifies the inflammatory response. Nat Immunol 15, 738–748 (2014). https://doi.org/10.1038/ni.2919

27. Dobre A, Nedelcu RI, Turcu G, Brinzea A, Struna I, et al. Multiple Keratoacanthomas Associated with Genetic Syndromes: Narrative Review and Proposal of a Diagnostic Algorithm. Am J Clin Dermatol [Internet]. 2024 [cited 2025 Apr 19];26:45. Available from: https://pmc.ncbi.nlm.nih.gov/articles/PMC11742465/

28. Schindelin J, Arganda-Carreras I, Frise E, Kaynig V, Longair M, Pietzsch T, et al. Fiji: An open-source platform for biological-image analysis. Nat Methods [Internet]. 2012 [cited 2025 Jul 16];9:676–82. Available from: https://www.nature.com/articles/nmeth.2019

29. Kremer JR, Mastronarde DN, McIntosh JR. Computer visualization of three-dimensional image data using IMOD. Journal of Structural Biology. 1996 Jan-Feb;116(1):71-76. DOI: 10.1006/jsbi.1996.0013. PMID: 8742726.

30. Ceafalan LC, Fertig TE, Gheorghe TC, Hinescu ME, Popescu BO, et al. Age-related ultrastructural changes of the basement membrane in the mouse blood-brain barrier. J Cell Mol Med [Internet]. 2019 [cited 2025 Jul 16];23:819–27. Available from: https://pubmed.ncbi.nlm.nih.gov/30450815/

484 **SUPPLEMENTARY**

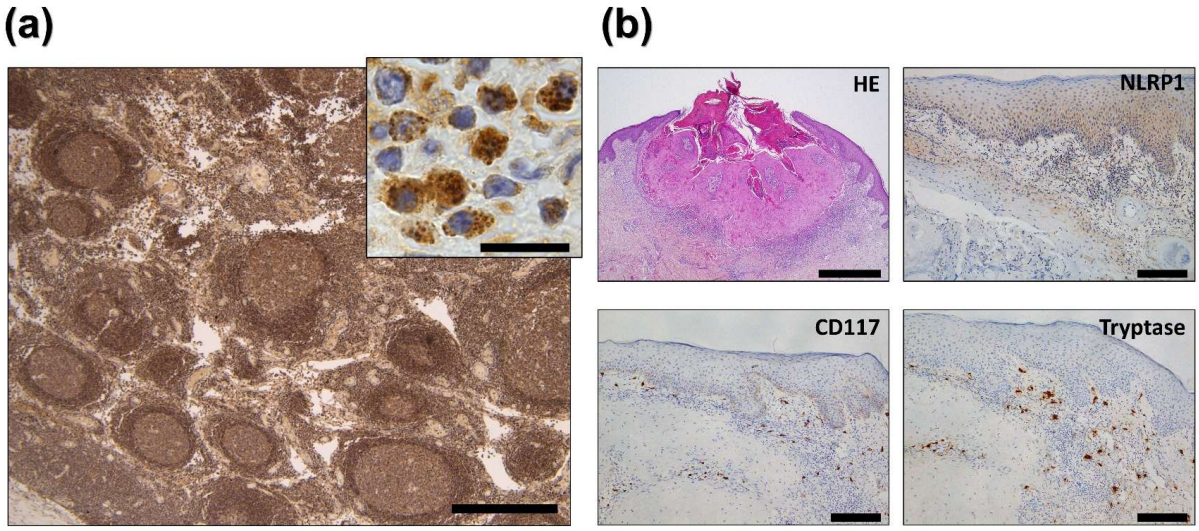

485 **Supplementary Figure S1. Additional immunohistochemistry controls for NLRP1**
486 **localization and for mast cell involvement in KA lesions. (a)** Human lymph node stained
487 against NLRP1, showing highest proportion of positive cells in the mantle zone of lymphoid
488 follicles. Scale bar = 500 µm. Higher magnification **(inset**, scale bar = 20 µm**)** demonstrates
489 localization of NLRP1 to granules of immune cells in lymph node. **(b)** Representative regions
490 from non-MSPC KA, under different stains, showing absence of mast cell degranulation and
491 epidermal infiltration. Scale bars are: 500 and 20 µm for (a) and inset, respectively; 1 mm for
492 HE staining in (b) and 200 µm for all others panels in (b).

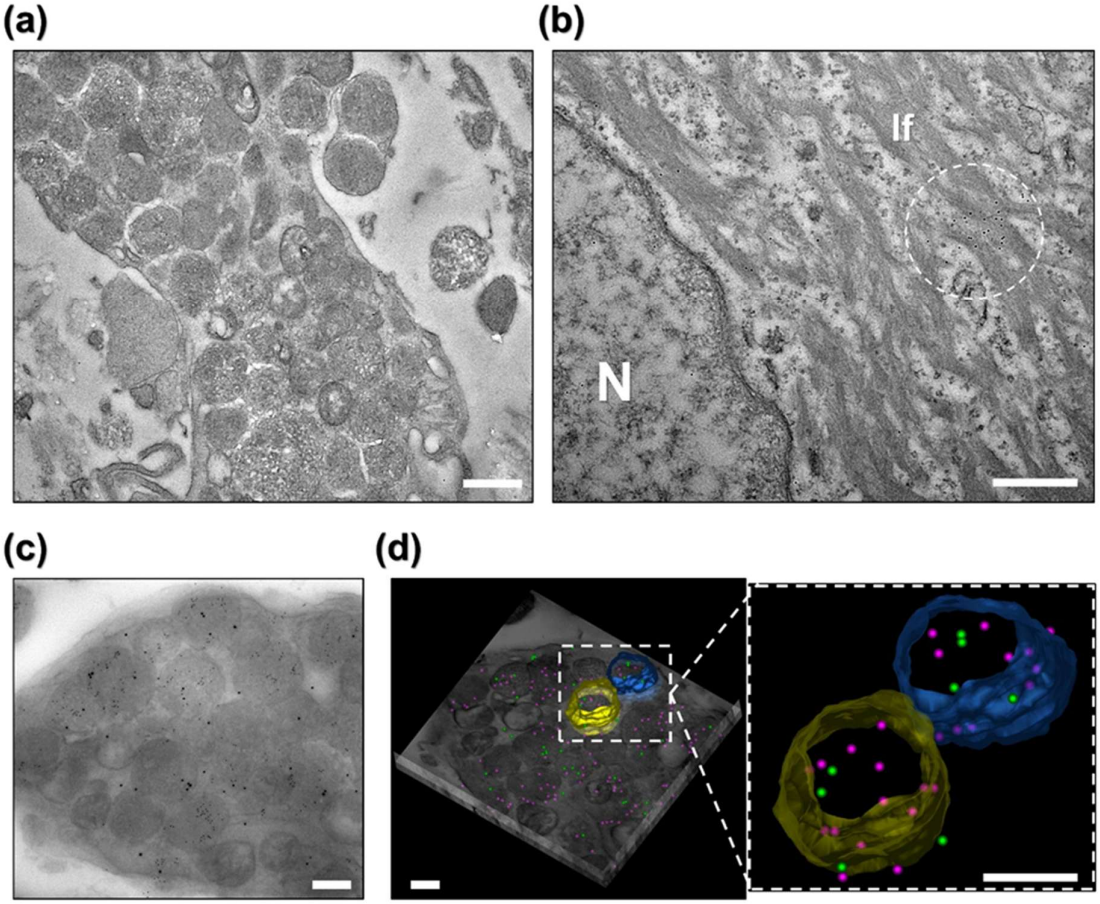

Supplementary Figure S2. Immunoelectron microscopy negative control and immunoelectron tomography of NLRP1 and NLRP3 colocalization in mast cell granules. **(a)** A rabbit isotype control did not significantly bind to mast cell (MC) granules. **(b)** NLRP1 localized to intermediate filaments (If) of keratinocytes. Representative accumulation of colloidal gold can be seen as black dots (circled area). *N - nucleus.* **(c)** Projection from tomographic tilt series, showing colocalization of 10 and 15 nm gold particles ($NLRP1^{A66V}$ and NLRP3, respectively) in granules from a MC in MSPC-KA. **(d)** Reconstructed tomogram with superimposed drawn contours of two MC granules (yellow and blue), presenting colocalization of $NLRP1^{A66V}$ (magenta) and NLRP3 (green). Detail of segmented MC granules demonstrating colocalization of $NLRP1^{A66V}$ (magenta) and NLRP3 (green) are presented in the boxed area. Scale bars = 500 nm.

504 **Video S1. NLRP1 and NLRP3 colocalize to MC granules in MSPC-KA.** In situ tomogram
505 and segmentation showing colocalization of NLRP1 (magenta) and NLRP3 (green) to MC
506 granules in MSPC-KA (related to Figure S3c,d).

507 **Video S2. NLRP1, NLRP3 and IL1β colocalize to MC granules in MSPC-KA.** In situ
508 tomogram and segmentation showing colocalization of NLRP1 (magenta), NLRP3 (turquoise)
509 and IL1β (green) to MC granules in MSPC-KA (related to Figure 4c-e). for (a-b).